J Nanopart Res (2017) 19: 187
DOI 10.1007/s11051-017-3884-9

RESEARCH PAPER

Magnetic porous PtNi/SiO2 nanofibers for catalytic hydrogenation of *p*-nitrophenol

Huijuan Guan · Cong Chao · Weixiao Kong · Zonggao Hu · Yafei Zhao · Siguo Yuan · Bing Zhang

Received: 16 January 2017 / Accepted: 4 May 2017 / Published online: 25 May 2017

Abstract In this work, the mesoporous SiO_2 nanofibers from pyrolyzing precursor of electrospun nanofibers were employed as support to immobilize PtNi nanocatalyst (PtNi/SiO_2 nanofibers). AFM, XRD, SEM, TEM, XPS, ICP-AES and N_2 adsorption/desorption analysis were applied to systematically investigate the morphology and microstructure of as-prepared products. Results showed that PtNi alloy nanoparticles with average diameter of 18.7 nm were formed and could be homogeneously supported on the surface of porous SiO_2 nanofiber, which further indicated that the SiO_2 nanofibers with well-developed porous structure, large specific surface area, and roughened surface was a benefit for the support of PtNi alloy nanoparticles. The PtNi/SiO_2 nanofibers catalyst exhibited an excellent catalytic activity towards the reduction of *p*-nitrophenol, and the catalyst's kinetic parameter ($k_n = 434 \times 10^{-3}$ mmol s^{-1} g^{-1}) was much higher than those of Ni/SiO_2 nanofibers (18×10^{-3} mmol s^{-1} g^{-1}), Pt/SiO_2 nanofibers (55×10^{-3} mmol s^{-1} g^{-1}) and previous reported PtNi catalysts. The catalyst could be easily recycled from heterogeneous reaction system based on its good magnetic properties (the Ms value of 11.48 emu g^{-1}). In addition, PtNi/SiO_2 nanofibers also showed an excellent stability and the conversion rate of *p*-nitrophenol still could maintain 94.2% after the eighth using cycle.

Keywords Porous SiO_2 nanofibers · PtNi alloy nanocatalyst · *p*-Nitrophenol · Hydrogenation reaction · Nanocomposites

Introduction

p-Nitrophenol is a type of highly toxic and potentially carcinogenic compound produced from versatile industries of explosive, pharmaceutical, pesticide, dye, pigment, rubber chemical and wood preservative process, and has been listed as priority pollutants due to its high toxicity and non-biodegradation (Bae et al. 2016; Chen et al. 2016; Sun and Lemley 2011). *p*-Aminophenol is an important intermediate for the fabrication of pharmaceuticals, photographic developers, anticorrosion lubricants and other industrially important products. Over the past few years, the heterogeneous catalytic reduction of *p*-nitrophenol to *p*-aminophenol by $NaBH_4$ in the aqueous solution was regarded as a green and sustainable manufacture process to dispose *p*-nitrophenol and produce *p*-aminophenol (Saha et al. 2010; Wu et al. 2011). Therefore, it is important to develop novel effective catalysts for the reaction.

In recent years, bimetallic nanocatalysts, especially Pt-based alloys, have been getting increased attentions due to their enhanced activity, stability and selectivity compared with pure metals in many heterogeneous catalytic processes. Pt-based alloys are kind of important catalyst systems and usually composed of Pt and transition metals, such as

Electronic supplementary material The online version of this article (doi:10.1007/s11051-017-3884-9) contains supplementary material, which is available to authorized users.

H. Guan · C. Chao · W. Kong · Z. Hu · Y. Zhao · S. Yuan · B. Zhang (✉)
School of Chemical Engineering and Energy, Zhengzhou University, Zhengzhou 450001, People's Republic of China
e-mail: zhangb@zzu.edu.cn

PtNi, PtFe, PtCu, PtCo, PtRu, and so on (Zou et al. 2015; Shukla et al. 2004; He and Li 1988; Ohkubo et al. 2013; Kageyama et al. 2011; Yang et al. 2016). The size and dispersion of Pt-based alloy nanoparticles make significant difference on their specific catalytic properties, and highly dispersed nanoparticles with small size and narrow size distribution usually show excellent catalytic performance owing to their large surface area and specific electronic structure. However, the Pt-based alloy nanoparticles are not stable and easy to aggregate because of their high surface energy, which subsequently leads to decline of their catalytic activity (Sahoo et al. 2014).

In order to solve the above problems, Pt-based alloy nanoparticles can be immobilized on the surface of supports with large surface area (Sahoo et al. 2014; Zhao et al. 2016). Nanostructured supports with various morphologies such as sphere, sheet, rod, tube and fiber have been used as novel supports to load metal catalysts (Hu and Chua 2016; Yoo et al. 2009; Li et al. 2012; Zhuang et al. 2016; Ogunlaja et al. 2016). Electrospinning is a promising, simple and low-cost strategy to produce fibers with diameters ranged from nanoscale to micrometer scale. The nanofibers, the products of pyrolysis from electrospun nanofibers, have been considered as an alternative for the support materials owing to their large surface area, controllable size, high mechanical strength and good stability (Guo et al. 2014). Previous research revealed that highly porous structure of nanofibers provided numerous attachment sites for nanocatalysts and also ensured the permeability of the support matrix and the accessibility of the reactant molecules (Fu et al. 2016; Lee et al. 2011; Zhao et al. 2008).

In the present work, we prepared mesoporous SiO_2 nanofibers by pyrolyzing precursor of SiO_2 electrospun nanofibers and then employed it as support to immobilize PtNi nanocatalyst. Characterization results showed that PtNi alloy nanoparticles could be homogeneously supported on the surface of SiO_2 nanofibers. PtNi/SiO_2 nanofibers showed superior catalytic activity and good reusability towards the reduction reaction of *p*-nitrophenol to *p*-aminophenol by $NaBH_4$ in the aqueous solution.

Materials and methods

Reagents and instruments

Polyvinylpyrrolidone (PVP, M_w = 1,300,000), tetraethyl orthosilicate (TEOS), anhydrous ethanol, $Ni(NO_3)_2{\cdot}6H_2O$, $H_2PtCl_6{\cdot}6H_2O$, NaOH, HCl, hydrazine hydrate, *p*-nitrophenol and $NaBH_4$ were all purchased from commercial suppliers and used without further purification. Double-distilled water was used throughout the experiment.

Atomic force microscopy (AFM) study was carried out using Bruck Dimension FastScan scanning probe microscope. N_2 adsorption/desorption isotherms and the corresponding pore size distribution were recorded on Quantachrome NOVA4200 specific surface area and pore size distribution analyzer. Field emission scanning electron microscopy (FE-SEM) images were observed by JEOL JSM-6701F FE-SEM. Transmission electron microscopy (TEM) images were taken using a JEOL JEM-2100 TEM. X-ray Powder Diffraction (XRD) data was obtained with a Rigaku Ultima III X-ray diffractometer. High-resolution X-ray photoelectron spectroscopy (XPS) was carried out on a VG ESCALAB250 X-ray photoelectron spectrometer. The composition of the catalyst was determined using Shimadzu ICPS-7500 inductively coupled plasma-atomic emission spectrometry (ICP-AES) technique. The magnetic measurement was performed using a Lake Shore 7404 vibrating sample magnetometer. The UV-Vis adsorption spectra were determined on UV-2450 UV-Vis spectrophotometer.

Preparation of porous SiO_2 nanofibers

For the preparation of TEOS spinning solution, PVP (3.0 g) and TEOS (3.0 g) were dissolved into anhydrous ethanol (30.0 mL) followed by being stirred for 2 h at 25 °C. Then, HCl (0.26 mL) was added dropwise into the above solution to control the hydrolysis/gelation of TEOS; this was followed by continuous stirring the system for 12 h. The electrospinning was performed under a positive high voltage of 20 kV with a solution feeding rate of 30 μL min^{-1}, and the distance between the collector and the tip of the needle was set as 15 cm. Subsequently, the as-electrospun nanofibrous mat was calcined at 550 °C in air for 2 h to obtain porous SiO_2 nanofibers.

Preparation of PtNi/SiO_2 nanofibers

SiO_2 nanofibers (0.28 g) were added into ethylene glycol (160 mL) and ultrasonicated for 1 h to form a stable suspension of SiO_2 nanofibers. $H_2PtCl_6{\cdot}6H_2O$ aqueous solution (0.03352 mol L^{-1}, 4.3 mL) and $Ni(NO_3)_2{\cdot}6H_2O$ (416.3 mg) were dissolved in ethylene glycol (40 mL). This metal salt solution was added into the above SiO_2 nanofiber suspension followed by

addition of hydrazine hydrate (85 wt%, 6.4 mL) and NaOH ethylene glycol solution (0.375 mol L^{-1}, 7.2 mL). This mixture was kept in an ultrasonic bath for 10 min and then stirred at 110 °C for 3 h under N_2 atmosphere. The above reaction suspension was cooled and subsequently separated by centrifugation. The prepared solid product was thoroughly washed with water and anhydrous ethanol and then dried in a vacuum oven at 50 °C for 24 h to obtain PtNi/SiO_2 nanofibers. For comparison, Pt/SiO_2 nanofibers and Ni/SiO_2 nanofibers were also prepared using the same method.

Catalytic reduction of *p*-nitrophenol

The reduction of *p*-nitrophenol into *p*-aminophenol by $NaBH_4$ is widely used as a model reaction for monitoring the catalytic activity of metal nanoparticles (Deka et al. 2017). So this reaction was adopted to quantitatively evaluate the catalytic activity of the as-prepared catalysts at 25 °C. In a typical procedure, freshly prepared *p*-nitrophenol aqueous solution (2×10^{-3} mol L^{-1}, 20 mL) and $NaBH_4$ aqueous solution (0.25 mol L^{-1}, 20 mL) were mixed to form a uniform solution by stirring for 2 min, and then SiO_2 nanofiber-supported nanocatalyst (5.0 mg) was added into the above solution. During the reaction process, the reaction solution (0.5 mL) was taken from the reaction system at a regular interval of 1 min, and subsequently diluted with double-distilled water (9.5 mL). The reaction process was monitored by measuring the change of UV-Vis absorbance intensity of *p*-nitrophenol at 400 nm. The sampling procedure was continued until the reaction solution became colorless. The reusability experiment was conducted by the same procedure.

Results and discussion

Characterization of the as-synthesized target products

Figure 1 shows the typical AFM images of SiO_2 nanofibers precursor and SiO_2 nanofibers. It could be observed that the precursor of SiO_2 nanofibers showed a smooth surface (Fig. 1a, c), while SiO_2 nanofibers revealed a rough and irregular surface (Fig. 1b, d). Surface roughness parameters of mean roughness (Ra) and root mean square roughness (Rq) were presented in Fig. 1. The Rq and Ra values for SiO_2 nanofibers (Rq = 21.02 nm, Ra = 17.10 nm) were three times higher than those of SiO_2 nanofibers precursor (Rq = 6.08 nm, Ra = 5.12 nm). The roughness variation of SiO_2 nanofibers could be attributed to the formation of porous structure on the surface due to pyrolyzing of precursor. The rough surface and porous structure could help catalyst nanoparticles to support uniformly on the surface of SiO_2 nanofibers.

Figure 2 shows the XRD patterns of Pt/SiO_2 nanofibers and PtNi/SiO_2 nanofibers. A broad diffraction peak at two theta in the range of 15–30° was corresponded to the amorphous SiO_2 (JCPDS 29-0085). For Pt/SiO_2 nanofibers, the diffraction peaks detected at around 40.0, 46.5, 68.0, and 81.5° were attributed to the (111), (200), (220) and (311) crystal planes of Pt face-centered cubic crystal structure (JCPDS 04-0802), respectively. Diffraction pattern of PtNi/SiO_2 nanofibers showed similar peaks as those of Pt/SiO_2 nanofibers. It is worth noting that the four diffraction peaks of PtNi/SiO_2 nanofibers were slightly shifted to higher 2 theta values with respect to those of Pt/SiO_2 nanofibers, which suggested the formation of PtNi alloy (Kim et al. 2009; Zhang et al. 2014a).

The porous structure of the obtained SiO_2 nanofibers and PtNi/SiO_2 nanofibers were characterized by N_2 adsorption/desorption analysis. SiO_2 nanofibers and PtNi/SiO_2 nanofibers exhibited type-IV adsorption isotherm pattern with hysteresis loop in the range of P/P_0 0.4–1.0 (Fig. 3a). According to the classification by the International Union of Pure and Applied Chemistry (IUPAC) (Leofanti et al. 1998), the shape of the hysteresis loop was identified as type-H1, corresponding to the narrow mesoporous pores within SiO_2 nanofibers and PtNi/SiO_2 nanofibers. The SiO_2 nanofibers had a specific Brunauer-Emmett-Teller (BET) surface area of 644.93 m^2 g^{-1} and average pore diameter of 3.8 nm. The large surface area of SiO_2 nanofibers provided an ample space for supporting of metal nanoparticles on their surface. However, the BET surface area and average pore diameter of PtNi/SiO_2 nanofibers were 351.37 m^2 g^{-1} and 3.4 nm, respectively. The declination of surface area and average pore diameter of PtNi/SiO_2 nanofibers could be attributed to the loading of metal nanoparticles and the blockage of mesopores by metal nanoparticles (Wang and Dai 2009).

To reveal the morphology and microstructure of SiO_2 nanofibers and PtNi/SiO_2 nanofibers, SEM, TEM and HRTEM observations were carried out in Fig. 4. It could be seen that one-dimensional SiO_2 nanofibers with average diameter of 400 nm were obtained in Fig. 4a. Compared with the SEM image of SiO_2 nanofibers

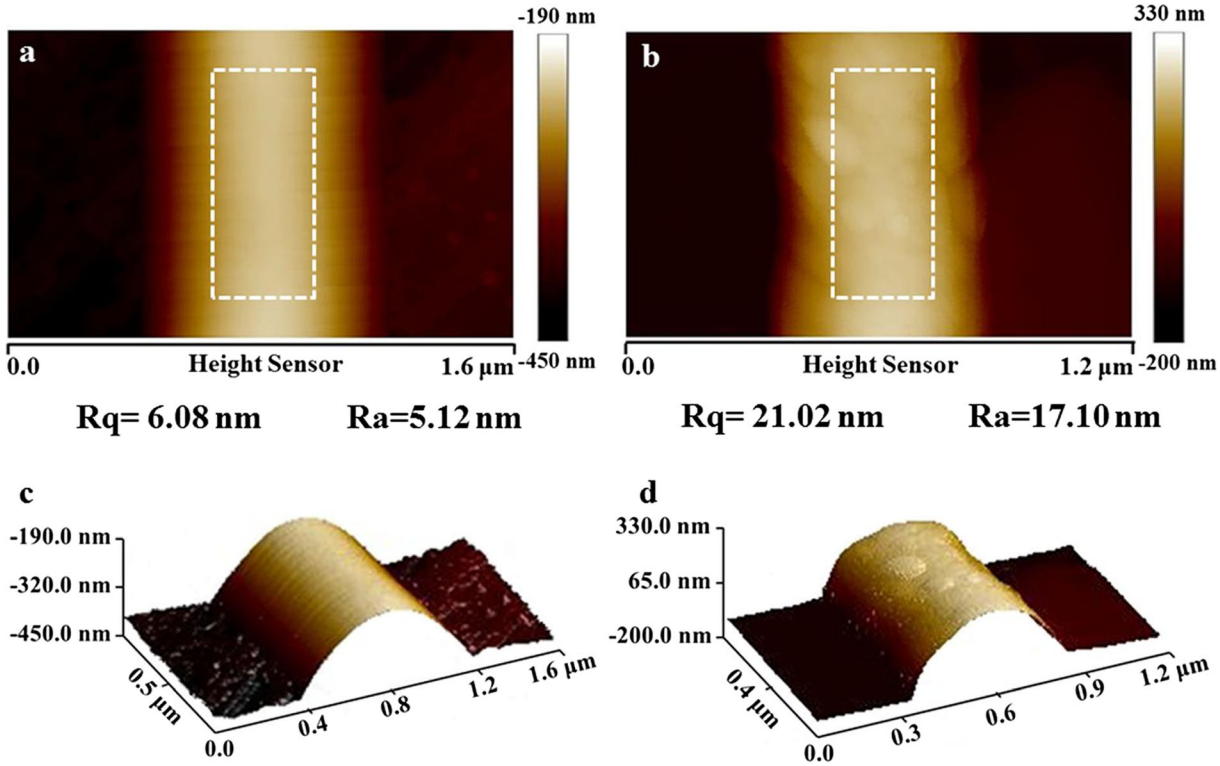

Fig. 1 Two-dimensional and three-dimensional AFM images of SiO_2 nanofibers precursor (**a, c**) and SiO_2 nanofibers (**b, d**)

precursor (Fig. S1), the enlarged SEM image of SiO_2 nanofibers (the inset of Fig. 4a) further revealed that the last pyrolysis process created a rough surface, which was in accordance with the results of AFM analysis. TEM image of $PtNi/SiO_2$ nanofibers showed that metal nanoparticles were successfully and uniformly loaded on the surface of SiO_2 nanofibers (Fig. 4b). The statistical result showed that distribution range of PtNi particles size was narrow and the average diameter of them was 18.7 nm (Fig. 4c). To further reveal the microstructure of PtNi nanoparticles, HRTEM observation was carried out. As shown in Fig. 4d, the lattice spacing of 0.214 nm was larger than that of the pure Ni (0.203 nm) and was smaller than that of the (111) plane of Pt (0.23 nm), which provided additional evidence for the formation of PtNi alloy (Bai et al. 2012; Zhang et al. 2010, and the lattice fringe was attributed to the (111) plane of face-centered cubic PtNi alloy (Zhu et al. 2016).

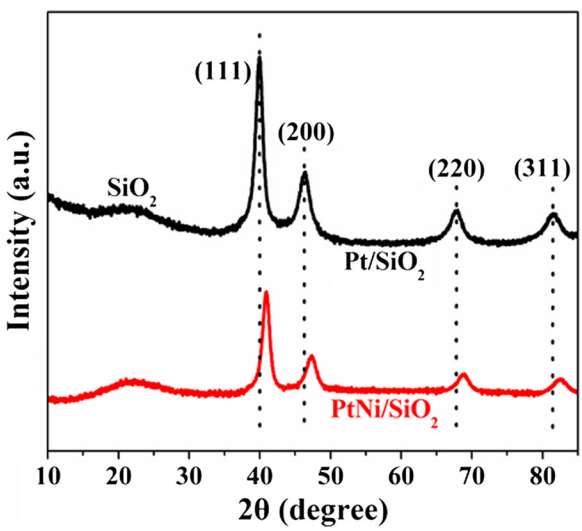

Fig. 2 XRD patterns of Pt/SiO_2 nanofibers and $PtNi/SiO_2$ nanofibers

The XPS measurement was used to evaluate the surface structure and chemical states of as-prepared catalysts. Figure 5a shows the XPS spectra of Pt4f in Pt/SiO_2 nanofibers and $PtNi/SiO_2$ nanofibers. It could be observed that Pt existed predominantly in Pt^0 form, demonstrating that Pt^{4+} precursor was successfully reduced to form metallic Pt on the surface of SiO_2 nanofibers. And the new strong peak at the binding energy value of 67.3 eV for $PtNi/SiO_2$ nanofibers could be assigned to the XPS peak of Ni3p (Ma et al. 2014). It

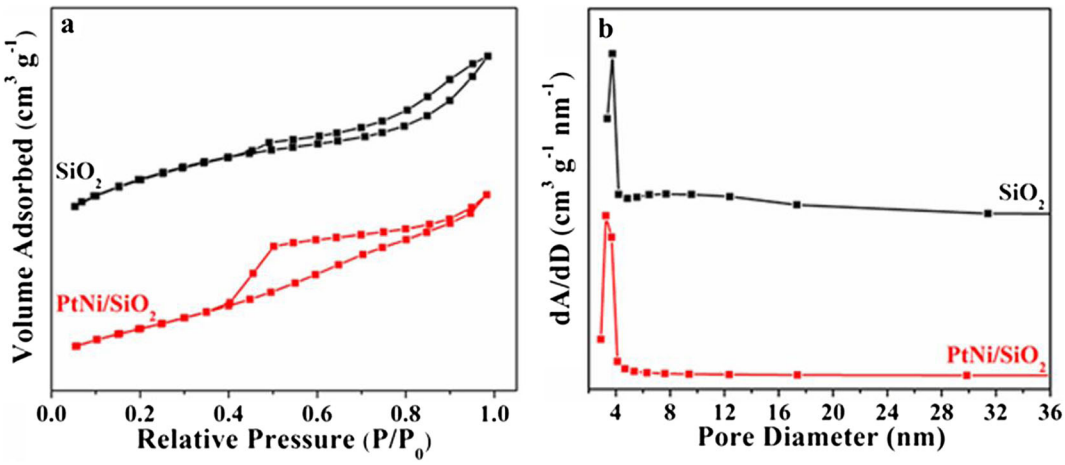

Fig. 3 N_2 adsorption/desorption isotherms (**a**) and the corresponding pore size distribution (**b**) of SiO_2 nanofibers and PtNi/SiO_2 nanofibers

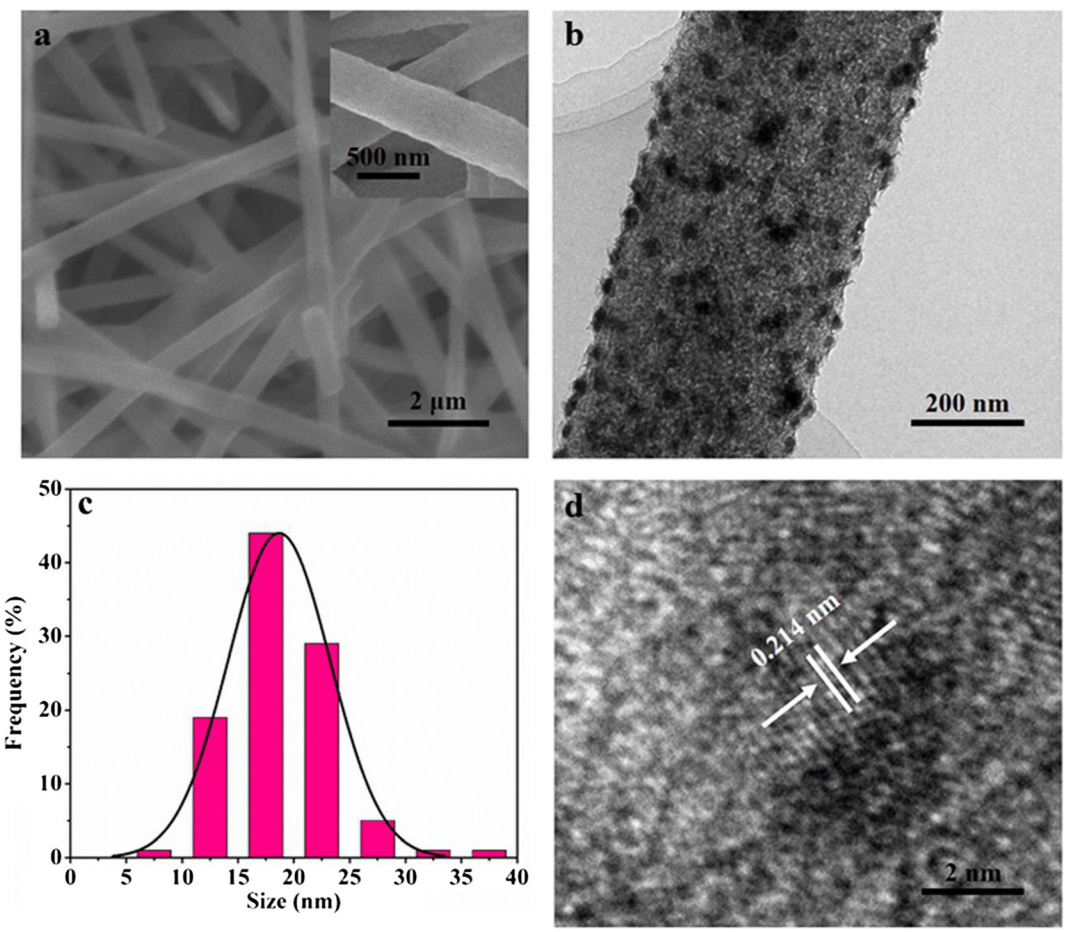

Fig. 4 SEM and enlarged SEM images of SiO_2 nanofibers (**a**), TEM image of PtNi/SiO_2 nanofibers (**b**), the size distribution of PtNi nanoparticles (**c**), and HRTEM lattice image of PtNi catalyst (**d**)

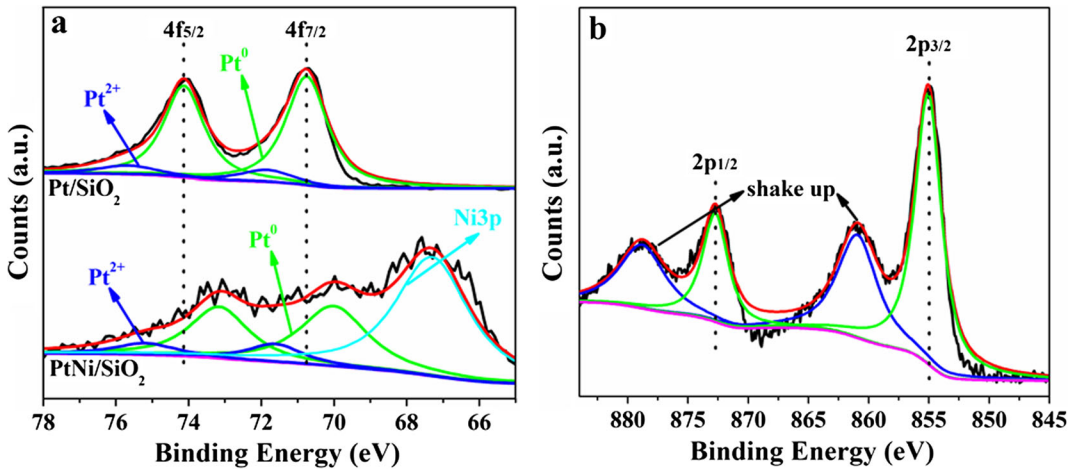

Fig. 5 The XPS spectra of Pt4f in Pt/SiO_2 nanofibers and $PtNi/SiO_2$ nanofibers (**a**) and the XPS spectra of Ni2p in $PtNi/SiO_2$ nanofibers (**b**)

is notable that the Pt4f peaks of $PtNi/SiO_2$ nanofibers showed negative shifts compared to those of Pt/SiO_2 nanofibers, which may be caused by the transfer of electrons from Ni to Pt in PtNi alloy (Sahoo et al. 2014). The electronic transfer can result in the downshift of the Pt d-band center position which plays a vital role in determining the catalytic performance. The downshift is directly related to the adsorption energies of the reactants on the catalyst as well as their activation barriers, which may be good for the improvement of catalytic activity (Ahmadi et al. 2015; Zhang et al. 2014b). In the fine spectra of Ni2p in $PtNi/SiO_2$ nanofibers (Fig. 5b), the peaks at the binding energies of 855.04 and 872.72 eV were ascribed to $Ni2p_{3/2}$ and $Ni2p_{1/2}$, respectively. Besides, there were two shake-up satellite signals caused by multi-electron excitation at 860.86 and 878.68 eV (Song et al. 2015a). These results were found to be in agreement with other literature values of PtNi alloys (Sahoo et al. 2014; Ahmadi et al. 2015; Shukla et al. 2001).

Catalytic activity of $PtNi/SiO_2$ nanofibers

The time-dependent UV-Vis absorption spectra changes of *p*-nitrophenol catalyzed by different catalysts are shown in Fig. 6. The UV-Vis absorption peak at 400 nm is the characteristic of *p*-nitrophenolate ions in alkaline solution (Ye et al. 2016). It was observed that the intensity of absorption peak at 400 nm almost had no change in the presence of pure SiO_2 nanofibers after 24 h of experimentation (Fig. 6a), indicating that SiO_2 nanofibers itself could not be used as catalyst and this reduction reaction could not proceed without catalyst. When Ni/SiO_2 nanofibers and Pt/SiO_2 nanofibers were added into the reaction system, the absorption peak intensity decreased gradually with time increase, and the conversion rates (%) of *p*-nitrophenol to *p*-aminophenol after 6 min for catalysts of Ni/SiO_2 nanofibers and Pt/SiO_2 nanofibers were 17.9 and 43.7%, respectively (Fig. 6b, c). Notably, $PtNi/SiO_2$ nanofibers showed the highest catalytic activity compared with Pt/SiO_2 nanofibers and Ni/SiO_2 nanofibers and can transform *p*-nitrophenol to *p*-aminophenol completely within 6 min (Fig. 6d). Moreover, the catalytic properties for the physical mixture of Pt/SiO_2 nanofibers and Ni/SiO_2 nanofibers (Pt/SiO_2 + Ni/SiO_2, with mass ratio of Pt/SiO_2:Ni/SiO_2 = 1:3) were measured. The result showed that the catalytic activity of Pt/SiO_2 + Ni/SiO_2 was far less than $PtNi/SiO_2$ nanofibers, and the conversion rate of *p*-nitrophenol to *p*-aminophenol only reached 52.4% at 6 min (Fig. S2). The simple physical mixture of Pt/SiO_2 + Ni/SiO_2 could not improve catalytic activity effectively and the excellent catalytic activity of $PtNi/SiO_2$ nanofibers could be attributed to the synthetic effect of Pt and Ni within PtNi alloy (Bae et al. 2012; Kang et al. 2016).

The kinetics of this reduction reaction was studied for evaluating the catalytic rate of different catalysts. It is usually followed the pseudo-first-order kinetics with respect to the concentration of *p*-nitrophenol (Song et al. 2015b), which is given as follows:

$$\ln\left(C_t/C_0\right) = \ln\left(A_t/A_0\right) = -k_a t \quad (1)$$

where C_t and C_0 represent the concentration of *p*-nitrophenol at times t and $t = 0$, respectively. A_t and A_0 are the

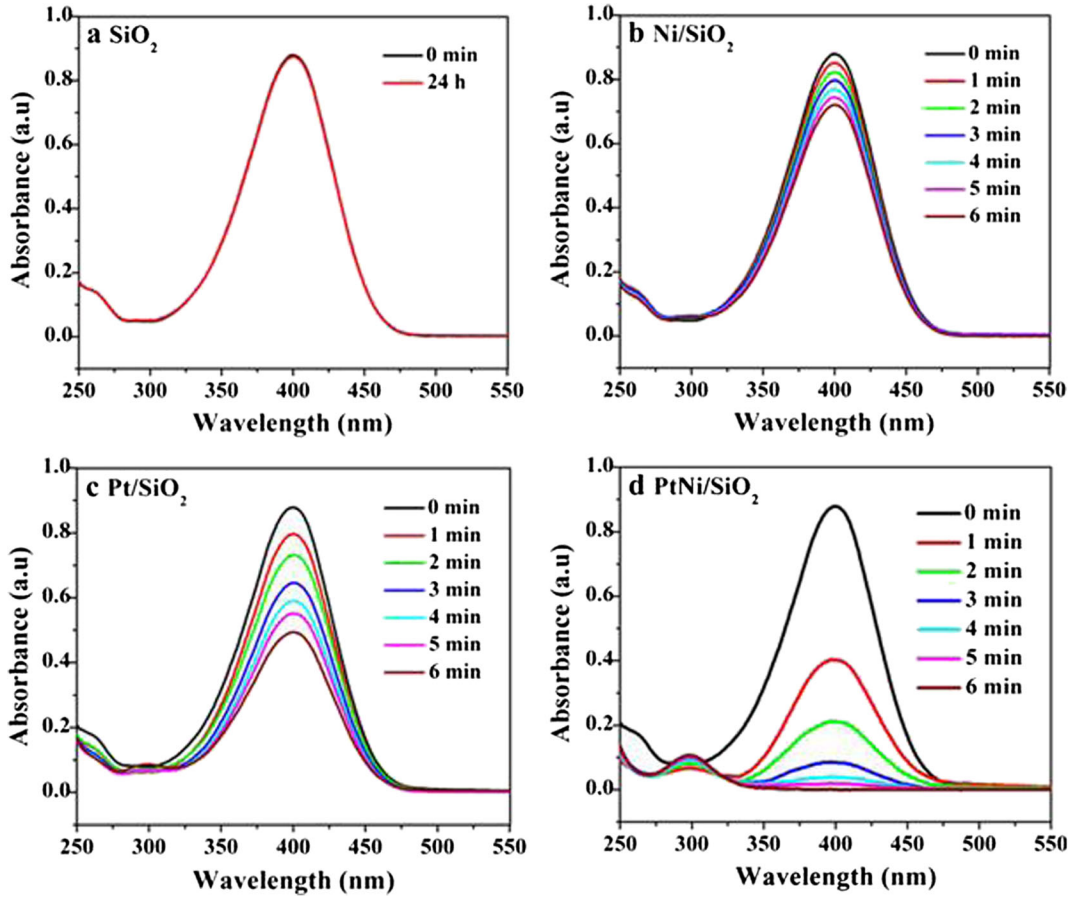

Fig. 6 Time-dependent UV-Vis adsorption spectra changes of *p*-nitrophenol for different catalysts

absorbance of *p*-nitrophenol (at peak of 400 nm) at times t and $t = 0$, respectively. k_a is the apparent rate constant. C_t/C_0 is calculated from A_t/A_0.

A linear relationship of $\ln(C_t/C_0)$ versus reaction time (t) was obtained in Fig. 7. The $\ln(C_t/C_0)$ showed a good linear correlation with the reaction time for all catalysts, which indicated that the reduction reaction of *p*-nitrophenol followed the pseudo-first-order kinetics. The k_a of different catalysts were calculated from the slopes of the linearly fitted plots of $\ln(C_t/C_0)$ versus time. The k_a values of Ni/SiO_2 nanofibers, Pt/SiO_2 nanofibers and PtNi/SiO_2 nanofibers for the reduction of *p*-nitrophenol were 0.55×10^{-3}, 1.61×10^{-3} and 12.84×10^{-3} s^{-1}, respectively.

In order to compare the catalytic activity with different catalysts of the previous reports, k_a should be further normalized to another comparable kinetic parameter, k_n, which can be defined as (Liu et al. 2013):

$$k_n = \left(10^{-3} C_0 V \Big/ m\right) k_a \quad (2)$$

where C_0 (mM) is the initial concentration of *p*-nitrophenol, V (mL) is the volume of reactant solution, and m (g) is

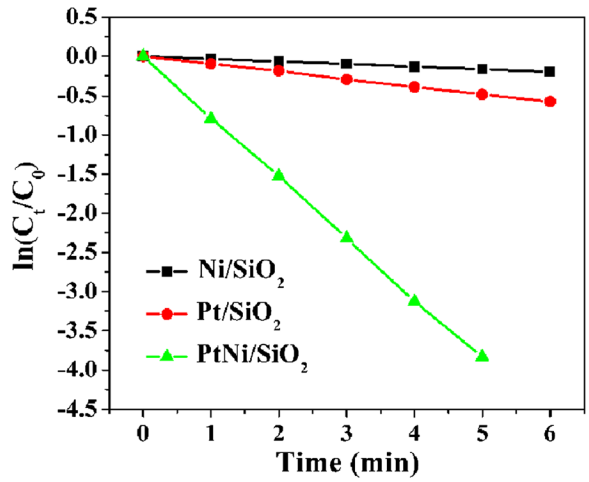

Fig. 7 Plots of $\ln(C_t/C_0)$ versus time in the presence of different catalysts

Table 1 Comparison of rate constant of $PtNi/SiO_2$ nanofibers with those of PtNi and supported PtNi nanocatalysts for *p*-nitrophenol reduction

Catalyst	Moles of *p*-nitrophenol	k_a/s^{-1}	k_n/mmol s^{-1} g^{-1}	Ref
$PtNi/SiO_2$ nanofibers	4×10^{-5} mol	12.84×10^{-3}	434×10^{-3}	This work
$Pt_{20}Ni_{80}$	2×10^{-7} mol	1.93×10^{-3}	45×10^{-3}	Ghosh et al. 2004
RGO/Pt-Ni (25:75)	1×10^{-5} mol	1.12×10^{-3}	–	Sahoo et al. 2014
PtNi nanosnowflakes/RGO	2.1×10^{-7} mol	2.17×10^{-3}	67×10^{-3}	Song et al. 2015b

the metal mass of catalyst. Based on the above formula and ICP-AES results (Table S1), the calculated k_n value of $PtNi/SiO_2$ nanofibers was 434×10^{-3} mmol s^{-1} g^{-1}, which was larger than those of Ni/SiO_2 nanofibers (18×10^{-3} mmol s^{-1} g^{-1}) and Pt/SiO_2 nanofibers (55×10^{-3} mmol s^{-1} g^{-1}). We compared the catalytic activity of $PtNi/SiO_2$ nanofibers with those of PtNi and supported PtNi nanocatalysts for *p*-nitrophenol reduction (Table 1) (Sahoo et al. 2014; Song et al. 2015b; Ghosh et al. 2004). The $PtNi/SiO_2$ nanofibers showed superior catalytic activity, and its k_n value was about 6.5 times higher than that of PtNi nanosnowflakes/RGO. The improved catalytic activity of $PtNi/SiO_2$ nanofibers was attributed to the following reasons: (1) the high surface area and porous structure of SiO_2 nanofibers benefited the adsorption of *p*-nitrophenol molecules, which helped reactant molecules to access the surface of catalyst; (2) the small size and uniform dispersion on the support surface of PtNi alloy nanocatalyst also contributed to the increasing of catalytic activity.

Recyclability and stability of $PtNi/SiO_2$ nanofibers

Magnetic property of $PtNi/SiO_2$ nanofibers was investigated at 25 °C using a vibrating sample magnetometer with an applied field $-18{,}000$ Oe < H < 18,000 Oe. The magnetic hysteresis loop of $PtNi/SiO_2$ nanofibers is shown in Fig. 8a. The $PtNi/SiO_2$ nanofibers exhibited typical ferromagnetic curve and its saturation magnetization (Ms) value was calculated to be 11.48 emu g^{-1}. Figure 8b shows the magnetic separation image of $PtNi/SiO_2$ nanofibers. When an external magnetic field was applied, the catalyst nanoparticles were attracted to the wall of vial and the suspension became clear and transparent, which indicated that $PtNi/SiO_2$ nanofibers could be easily recollected from reaction systems by an external magnet.

The stability of a catalyst is an important characteristic for practical applications. So the stability of $PtNi/SiO_2$ nanofibers was also evaluated for the reduction of *p*-nitrophenol. Figure 9 shows the conversion

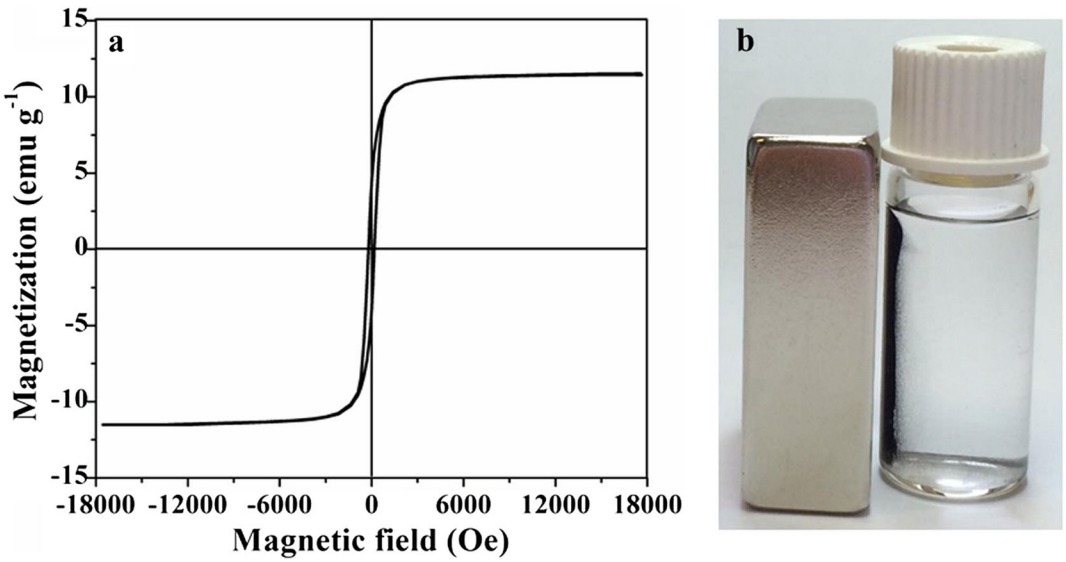

Fig. 8 Magnetic hysteresis loop of $PtNi/SiO_2$ nanofibers measured at 25 °C (**a**) and magnetic separation image of $PtNi/SiO_2$ nanofibers (**b**)

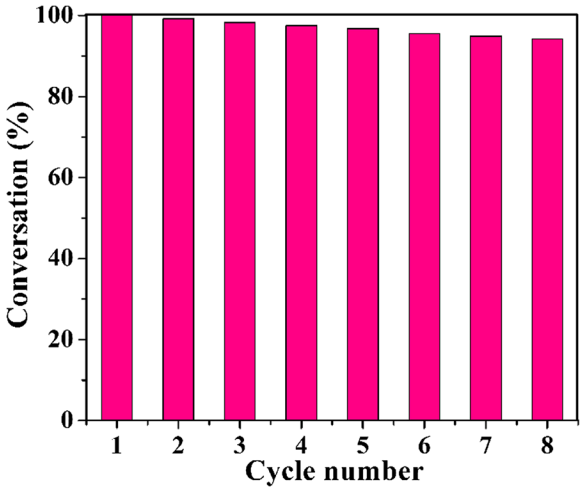

Fig. 9 Conversion rates of *p*-nitrophenol with PtNi/SiO_2 nanofibers as catalyst in eight successive cycles

rates of *p*-nitrophenol with PtNi/SiO_2 nanofibers as catalyst in eight successive cycles at 6 min. It could be seen that the conversion rate value slightly decreased with the increase of the cycle number, and the conversion rate of *p*-nitrophenol still could maintain 94.2% at the eighth cycle, which indicated that PtNi/SiO_2 nanofibers possessed excellent stability. This may be attributed to the strong nanocatalyst-support interaction strengthened by the rough surface of SiO_2 nanofibers, which contributed significantly to anchoring nanoparticles and protected them from leaching in recycling process.

Conclusion

In summary, PtNi alloy nanoparticles were homogeneously supported on the surface of porous SiO_2 nanofibers to form PtNi/SiO_2 nanofibers. The as-prepared PtNi/SiO_2 nanofibers exhibited highly catalytic activity towards the reduction of *p*-nitrophenol when only trace amount of PtNi catalyst was used. In addition, the catalyst could be easily recycled from heterogeneous reaction system based on its good magnetic properties; it also had excellent stability and still could maintain high catalytic activity for eight cycles. Considering its high catalytic activity, good recycling and excellent stability, the PtNi/SiO_2 nanofibers has promising applications in the area of advanced heterogeneous catalysis.

Acknowledgements This study was funded by the National Natural Science Foundation of China (21576247 and 21271158).

Compliance with ethical standards

Conflict of interest The authors declare that they have no conflict of interest.

References

Ahmadi M, Cui C, Mistry H, Strasser P, Cuenya BR (2015) Carbon monoxide-induced stability and atomic segregation phenomena in shape-selected octahedral PtNi nanoparticles. ACS Nano 9:10686–10694. doi:10.1021/acsnano.5b01807

Bae S, Gim S, Kim H, Hanna K (2016) Effect of $NaBH_4$ on properties of nanoscale zero-valent iron and its catalytic activity for reduction of *p*-nitrophenol. Appl Catal B-Environ 182:541–549. doi:10.1016/j.apcatb.2015.10.006

Bae SE, Gokcen D, Liu P, Mohammadi P, Brankovic SR (2012) Size effects in monolayer catalysis-model study: Pt submonolayers on Au(111). Electrocatalysis-US 3:203–210. doi:10.1007/s12678-012-0082-5

Bai S, Shen XP, Zhu GX, Xu Z, Yang J (2012) In situ growth of FeNi alloy nanoflowers on reduced graphene oxide nanosheets and their magnetic properties. CrystEngComm 14: 1432–1438. doi:10.1039/C1CE05916E

Chen X, Murugananthan M, Zhang Y (2016) Degradation of *p*-Nitrophenol by thermally activated persulfate in soil system. Chem Eng J 283:1357–1365. doi:10.1016/j.cej.2015.08.107

Deka P, Bhattacharjee D, Sarmah P, Deka RC, Bharali P (2017) Catalytic reduction of water contaminant '4-Nitrophenol' over manganese oxide supported Ni nanoparticles. In: Kurisu F, Ramanathan AL, Kazmi AA, Kumar M (eds) Trends in Asian water environmental science and technology. Springer International Publishing, New Delhi, pp 35–48

Fu K, Wang Y, Mao LC, Jin JH, Yang SL et al (2016) Facile one-pot synthesis of graphene-porous carbon nanofibers hybrid support for Pt nanoparticles with high activity towards oxygen reduction. Electrochimi Acta 215:427–434. doi:10.1016/j.electacta.2016.08.111

Guo QH, Liu D, Zhang XP, Li LB, Hou HQ et al (2014) Pd-Ni alloy nanoparticle/carbon nanofiber composites: preparation, structure, and superior electrocatalytic properties for sugar analysis. Anal Chem 86:5898–5905. doi:10.1021/ac500811j

Ghosh SK, Mandal M, Kundu S, Nath S, Pal T (2004) Bimetallic Pt-Ni nanoparticles can catalyze reduction of aromatic nitro compounds by sodium borohydride in aqueous solution. Appl Catal A-Gen 268:61–66. doi:10.1016/j.apcata.2004.03.017

Hu Y, Chua DHC (2016) Synthesizing 2D MoS_2 nanofins on carbon nanospheres as catalyst support for proton exchange membrane fuel cells. Sci Rep-UK 6:28088. doi:10.1038/srep28088

He HC, Li YN (1988) The phase transformations and structure of $Cu_{83.34}Pt_{16.86}$ alloy. J Mater Sci 23:1558–1562. doi:10.1007/BF01115691

Kim HJ, Choi SM, Nam SH, Seo MH, Kim WB (2009) Carbon-supported PtNi catalysts for electrooxidation of cyclohexane to benzene over polymer electrolyte fuel cells. Catal Today 146:9–14. doi:10.1016/j.cattod.2008.11.012

Kageyama S, Seino S, Nakagawa T, Nitani H, Ueno K et al (2011) Formation of PtRu alloy nanoparticle catalyst by radiolytic process assisted by addition of dl-tartaric acid and its enhanced methanol oxidation activity. J Nanopart Res 13:5275. doi:10.1007/s11051-011-0513-x

Kang YS, Yoo SJ, Lee MJ, Kim MJ, Lee SY et al (2016) Facile synthesis of platinum alloy electrocatalyst via aluminum reducing agent and the effect of post heat treatment for oxygen reduction reaction. Int J Hydrogen Energ 41: 22953–22962. doi:10.1016/j.ijhydene.2016.09.147

Lee JB, Jeong SI, Bae MS, Yang DH, Heo DN et al (2011) Highly porous electrospun nanofibers enhanced by ultrasonication for improved cellular infiltration. Tissue Eng Part A 17: 2695–2702. doi:10.1089/ten.TEA.2010.0709

Leofanti G, Padovan M, Tozzola G, Venturelli B (1998) Surface area and pore texture of catalysts. Catal Today 41:207–219. doi:10.1016/S0920-5861(98)00050-9

Li XH, Wang X, Antonietti M (2012) Mesoporous g-C_3N_4 nanorods as multifunctional supports of ultrafine metal nanoparticles: hydrogen generation from water and reduction of nitrophenol with tandem catalysis in one step. Chem Sci 3: 2170–2174. doi:10.1039/C2SC20289A

Liu J, Wu Q, Huang F, Zhang H, Xu S et al (2013) Facile preparation of a variety of bimetallic dendrites with high catalytic activity by two simultaneous replacement reactions. RSC Adv 3:14312–14321. doi:10.1039/C3RA41268G

Ma Y, Wang R, Wang H, Linkov V, Ji S (2014) Evolution of nanoscale amorphous, crystalline and phase-segregated PtNiP nanoparticles and their electrocatalytic effect on methanol oxidation reaction. Phys Chem Chem Phys 16:3593–3602. doi:10.1039/c3cp54600d

Ohkubo Y, Hamaguchi Y, Seino S, Nakagawa T, Kageyama S et al (2013) Preparation of carbon-supported PtCo nanoparticle catalysts for the oxygen reduction reaction in polymer electrolyte fuel cells by an electron-beam irradiation reduction method. J Mater Sci 48:5047–5054. doi:10.1007/s10853-013-7292-y

Ogunlaja AS, Kleyi PE, Walmsley RS, Tshentu ZR (2016) Nanofiber-supported metal-based catalysts. ACS Catal 28: 144–174. doi:10.1039/9781782626855-00144

Song P, Feng JJ, Zhong SX, Huang SS, Chen JR et al (2015a) Correction: facile preparation of reduced graphene oxide supported PtNi alloyed nanosnowflakes with high catalytic activity. RSC Adv 5:45641–45641. doi:10.1039/C5RA02681D

Song P, Feng JJ, Zhong SX, Huang SS, Chen JR et al (2015b) Facile preparation of reduced graphene oxide supported PtNi alloyed nanosnowflakes with high catalytic activity. RSC Adv 5:35551–35557. doi:10.1039/C5RA02681D

Sun SP, Lemley AT (2011) *p*-Nitrophenol degradation by a heterogeneous fenton-like reaction on nano-magnetite: process optimization, kinetics, and degradation pathways. J Mol Catal A-Chem 349:71–79. doi:10.1016/j.molcata.2011.08.022

Shukla AK, Neergat M, Bera P, Jayaram V, Hegde MS (2001) An XPS study on binary and ternary alloys of transition metals with platinized carbon and its bearing upon oxygen electroreduction in direct methanol fuel cells. J Electroanal Chem 504:111–119. doi:10.1016/S0022-0728(01)00421-1

Sahoo PK, Panigrahy B, Bahadur D (2014) Facile synthesis of reduced graphene oxide/Pt-Ni nanocatalysts: their magnetic and catalytic properties. RSC Adv 4:48563–48571. doi:10.1039/C4RA07686A

Saha S, Pal A, Kundu S, Basu S, Pal T (2010) Photochemical green synthesis of calcium-alginate-stabilized Ag and Au nanoparticles and their catalytic application to 4-nitrophenol reduction. Langmuir 26:2885–2893. doi:10.1021/la902950x

Shukla AK, Raman RK, Choudhury NA, Priolkarb KR, Sarodeb PR et al (2004) Carbon-supported Pt-Fe alloy as a methanol-resistant oxygen-reduction catalyst for direct methanol fuel cells. J Electroanal Chem 563:181–190. doi:10.1016/j.jelechem.2003.09.010

Wang X, Dai S (2009) A simple method to ordered mesoporous carbons containing nickel nanoparticles. Adsorption 15:138–144. doi:10.1007/s10450-009-9164-y

Wu KL, Wei XW, Zhou XM, Wu DH, Liu XW et al (2011) $NiCo_2$ alloys: controllable synthesis, magnetic properties, and catalytic applications in reduction of 4-Nitrophenol. J Phys Chem C 115:16268–16274. doi:10.1021/jp201660w

Yang H, Bradley SJ, Chan A, Waterhouse GIN, Nann T et al (2016) Catalytically active bimetallic nanoparticles supported on porous carbon capsules derived from metal-organic framework composites. J Am Chem Soc 138:11872–11881. doi:10.1021/jacs.6b06736

Yoo E, Okata T, Akita T, Kohyama M, Nakamura J et al (2009) Enhanced electrocatalytic activity of Pt subnanoclusters on graphene nanosheet surface. Nano Lett 9:2255–2259. doi:10.1021/nl900397t

Ye H, Wang Q, Catalano M, Lu N, Vermeylen J et al (2016) Ru nanoframes with an fcc structure and enhanced catalytic properties. Nano Lett 16:2812–2817. doi:10.1021/acs.nanolett.6b00607

Zou LL, Fan J, Zhou Y, Wang CM, Li J et al (2015) Conversion of PtNi alloy from disordered to ordered for enhanced activity and durability in methanol-tolerant oxygen reduction reactions. Nano Res 8:2777–2788. doi:10.1007/s12274-015-0784-0

Zhuang ZB, Giles SA, Zheng J, Jenness GR, Caratzoulas S et al (2016) Nickel supported on nitrogen-doped carbon nanotubes as hydrogen oxidation reaction catalyst in alkaline electrolyte. Nat Commun 7:10141. doi:10.1038/ncomms10141

Zhang CL, Hwang SY, Trout A, Peng ZM (2014a) Solid-state chemistry-enabled scalable production of octahedral Pt-Ni alloy electrocatalyst for oxygen reduction reaction. J Am Chem Soc 136:7805–7808. doi:10.1021/ja501293x

Zhao GW, He JP, Zhang CX, Zhou JH, Chen X et al (2008) Highly dispersed Pt nanoparticles on mesoporous carbon nanofibers prepared by two templates. J Phys Chem C 112:1028–1033. doi:10.1021/jp075116x

Zhao F, Kong WX, Hu ZG, Liu JD, Zhao YF et al (2016) Tuning the performance of Pt-Ni alloy/reduced graphene oxide catalysts for 4-nitrophenol reduction. RSC Adv 6:79028–79036. doi:10.1039/C6RA16045J

Zhu EB, Li YJ, Chiu CY, Huang XQ, Li MF et al (2016) In situ development of highly concave and composition-confined PtNi octahedra with high oxygen reduction reaction activity and durability. Nano Res 9:149–157. doi:10.1007/s12274-015-0927-3

Zhang P, Li R, Huang Y, Chen Q (2014b) A novel approach for the in situ synthesis of Pt-Pd nanoalloys supported on Fe_3O_4@C core-shell nanoparticles with enhanced catalytic activity for

reduction reactions. ACS Appl Mater Inter 6:2671–2678. doi:10.1021/am405167h

Zhang H, Yin YJ, Hu YJ, Li CY, Wu P et al (2010) Pd@Pt core-shell nanostructures with controllable composition synthesized by a microwave method and their enhanced electrocatalytic activity toward oxygen reduction and methanol oxidation. J Phys Chem C 27:11861–11867. doi:10.1021/jp101243k